TÜBİTAK

Turkish Journal of Physics

http://journals.tubitak.gov.tr/physics/

Research Article

Turk J Phys
(2018) 42: 210 – 222

doi:10.3906/fiz-1711-10

Monte Carlo simulation of dynamic phase transition properties of core-shell magnetic nanoparticles with similar volumes

Erol VATANSEVER*
Department of Physics, Faculty of Science, Dokuz Eylül University, İzmir, Turkey

Received: 11.11.2017 • **Accepted/Published Online:** 09.12.2017 • **Final Version:** 26.04.2018

Abstract: We implement Monte Carlo simulations to determine dynamic phase transition features of both cubical and spherical nanoparticles composed of spin-1/2 cores surrounded by a spin-1 shell layer. The particles are subjected to an oscillating magnetic field. We plan these particles such that they have similar volumes. It is observed that the nonequilibrium magnetic phase transition temperatures of the particles with similar volumes explicitly depend on their geometrical shapes as well as the system parameters. The cubic one has a higher transition temperature than the spherical one for the small interface coupling, whereas the transition temperature of the spherical particle becomes higher than that of the cubic one with further increment in antiferromagnetic coupling. We also analyze the magnetic features of the particles, such as dynamic remanence and coercivity treatments. Our simulation results suggest that the spherical particle has almost the same coercivity behavior as the cubic one for some considered system parameters. However, there are some differences in the context of remanence behaviors between spherical and cubic core-shell nanoparticles.

Key words: Core-shell cubical and spherical nanoparticles, dynamic phase transitions, Monte Carlo simulations

1. Introduction

Based on the developments in chemical synthesis techniques, scientists can now produce various types of controllable nanomaterials such as nanowires, nanotubes, nanorods, nanocubes, and other more complex shapes [1–10]. Nanoparticles are important materials that show unusual and interesting physical properties [11], and they are also potential candidates for applications in advanced nanotechnology [12–15] due to their distinctive magnetic properties. For example, multifunctionality core-shell nanowires have been produced by making use of a facile low-cost fabrication process, and it has been shown that a multidomain state at remanence can be obtained, which is an important and attractive feature for biomedical applications [14]. Recently, it has been reported that nanoparticles exhibit superparamagnetism [16], quantum tunneling of magnetization [17], and large coercivities [18]. It can also be said that one of the most interesting features of core-shell magnetic nanoparticles is the exchange bias phenomenon [19,20]. From the theoretical point of view, equilibrium phase transition properties of a great number of magnetic nanoparticle systems have been studied by benefiting from some methods such as mean field approximation (MFA) [21–24], effective field theory (EFT) [24–27], Green's function formalism [28,29], and Monte Carlo (MC) simulations [20–22,30–38].

We know today that an interacting spin system under the influence of a time-dependent oscillating magnetic field exhibits two important phenomena: dynamic phase transitions and hysteresis behavior. These types of magnetic systems attract the attention of the scientific community because they present unusual

*Correspondence: erol.vatansever@deu.edu.tr

and interesting dynamic behaviors. For instance, detailed numerical simulation studies reported that the universality classes of the Ising model and its variations under a time-dependent driving field are different from its equilibrium counterparts [39–41]. It is possible to emphasize that nonequilibrium phase transitions originate from a competition between time scales of the relaxation time of the system and oscillating period of the external applied field. For high temperatures and amplitudes of the external field, a simple ferromagnetic (FM) system exists in a dynamically disordered phase where time-dependent magnetization can follow the external magnetic field with some delay, whereas this is not the case for low temperature regions and small magnetic field amplitudes. The physical mechanism described above points out the existence of a dynamic symmetry-breaking phenomenon [39,42,43].

From the theoretical perspective, external field dependency of a FM system was first performed by Tomè and Oliveira by utilizing the kinetic mean field equation of motion [42]. From that time, many studies dealing with dynamic phase transitions and hysteresis properties of bulk as well as nanoparticle systems driven by a time-dependent magnetic field have been analyzed by a variety of techniques such as the MC simulation method [43–52], MFA [39,44,47,53,54], and EFT [55–58]. For example, in Refs. [56,57], thermal variations of time-averaged magnetizations, dynamic correlations between time-dependent magnetic fields and magnetization, and hysteresis loop areas of cylindrical Ising nanowire and nanotube systems have been elucidated by benefiting from Glauber-type stochastic processes [59]. It is underlined that, depending on the Hamiltonian parameters, the considered systems represent different types of magnetization profiles according to the Nèel theory of ferrimagnetism [60,61]. Moreover, a comprehensive MC simulation study with local spin update Metropolis algorithm has been carried out to determine the dynamic phase transitions, hysteresis, and finite size properties of a ferrimagnetic nanoparticle system with a core/shell structure [50]. It was reported that the system may exhibit a transition from a disordered to an ordered phase via tunable shell thickness. Recently, a spherical core/shell nanoparticle system with a spin-3/2 core coated by a spin-1 shell layer with antiferromagnetic (AFM) interface coupling was exposed to a sinusoidal magnetic field [51]. It was reported that dynamic phase boundaries strongly depend on the Hamiltonian parameters; for instance, for high amplitude and period of the external field, phase transition temperature sharply changes, whereas it tends to slowly alter as the reduced magnitude of interlayer coupling increases. Additionally, it was observed that the magnetization curves of the particle obeyed P-type, N-type, and Q-type classification schemes under certain conditions [51]. However, geometrical shape dependencies of nanoparticle systems on dynamic phase transition properties were not analyzed in the above cited studies. An open and interesting question is whether the dynamic phase transition properties of different shapes of magnetic nanoparticles with similar volumes are the same or not. As far as we know, by making use of equilibrium statistic mechanical and experimental tools, a limited number of studies have been dedicated to looking for an answer for this question [38,62–68]. For example, by combining a nonhydrolytic reaction with seed-mediated growth, it was reported that the values of T_B (blocking temperature) and of saturation magnetization of a spherical particle were larger than the cubic ones [62]. Recently, it was found by benefiting from both experimental and theoretical techniques that the value of T_B of maghemite particles depends on their geometrical structures, with spherical particles exhibiting larger T_B [68].

Based on the previously published works mentioned above, it is obvious that magnetic phase transition properties in equilibrium of differently shaped fine particles are clearly indicated. However, the understanding of the physics behind the nanoparticles under a time-dependent field deserves particular attention. From this point of view, we intend to investigate the nonequilibrium phase transition properties of cubical and spherical nanoparticles with similar volumes.

The paper is organized as follows: we give formulation and simulation details in Section 2. The results and discussion are given in Section 3, and finally Section 4 contains conclusions.

2. Formulation

We consider cubical and spherical magnetic nanoparticles composed of a spin-1/2 FM core that is coated by a spin-1 FM shell layer. The systems are located on the simple cubic lattice (for schematic representations, see Figure 1). At the interface of each particle, we use an AFM spin-spin coupling between core and shell spins. To keep the volumes of particles similar, one can select the total radius of spherical nanoparticles as R = 10 and the total thickness of cubical nanoparticles as L = 16. The particles are exposed to a magnetic field that oscillates in time. The Hamiltonian can be given as follows:

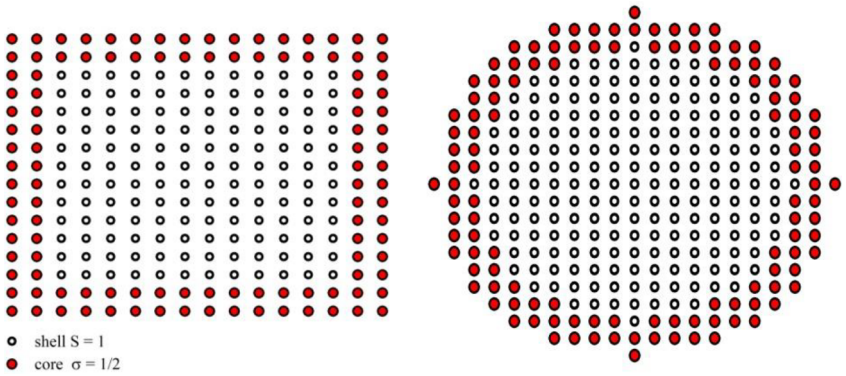

Figure 1. Schematic representations of the cubical and spherical core/shell nanoparticles with a spin-1/2 core and spin-1 shell.

$$\hat{H} = -J_{int} \sum_{\langle ik \rangle} \sigma_i S_k - J_c \sum_{\langle ij \rangle} \sigma_i \sigma_j - J_{sh} \sum_{\langle kl \rangle} S_k S_l - h(t) \left(\sum_i \sigma_i + \sum_k S_k \right) \tag{1}$$

where $\sigma = \pm 1/2$ and $S = \pm 1,\ 0$ are the spin variables in the core and shell sublattices of the systems. J_{int}, J_c, and J_{sh} describe the AFM interface $(J_{int} < 0)$, FM core $(J_c > 0)$, and FM shell $(J_{sh} > 0)$ spin-spin couplings, respectively. $h(t) = h_0 \sin(wt)$ shows the time-dependent magnetic field, where h_0 and w are the amplitude and the angular frequency of the field, respectively, and t is the time. The period of the field is $\tau = 2\pi/w$. The symbols $\langle \cdots \rangle$ shown in Eq. (1) denote the nearest neighbor interactions on the core/shell nanoparticle system. For the sake of simplicity, $J_{sh} = 1.0$ throughout the study.

We use MC simulations with the Metropolis algorithm [69], applying free boundary conditions in all directions for cubical and spherical particles. We note that application of such type of boundary conditions to the systems allows us to study the physics of the finite-size system. Readers can refer to reference [51] for details of the simulation procedure. Total number of the computer experiments is 50, and the total length of the simulation is 3×10^4 MC steps per site after discarding the first steps. We use the jackknife technique to calculate the error bars [70].

The time-dependent sublattice magnetizations, $M_c(t)$ and $M_{sh}(t)$, and the total magnetization $M(t)$ at

time t can be given as:

$$M_c(t) = \frac{1}{N_c}\sum_{i=1}^{N_c}\sigma_i(t), \quad M_{sh}(t) = \frac{1}{N_{sh}}\sum_{i=1}^{N_{sh}}S_i(t), \; M(t) = \frac{N_c M_c(t) + N_{sh}M_{sh}(t)}{N_c + N_{sh}} \tag{2}$$

where N_c and N_{sh} represent the total number of spins located in the core and shell layers, respectively. These numbers are $N_c = L_c^3 = 12^3$ and $N_{sh} = L^3 - L_c^3 = 16^3 - 12^3$ for cubic particles while they are $N_c = 2169\,(R_c = 8)$ and $N_{sh} = 2060\,(R_{sh} = 2)$ for spherical particles, respectively. From the time-dependent magnetizations, the dynamic order parameters can be obtained as follows:

$$Q_c = \frac{w}{2\pi}\oint M_c(t)\,dt, \quad Q_{sh} = \frac{w}{2\pi}\oint M_{sh}(t)\,dt, \quad Q = \frac{w}{2\pi}\oint M(t)dt, \tag{3}$$

where $Q_c \quad Q_{sh}$, and Q correspond to the dynamic order parameters. From this point of view, we can also use two additional order parameters belonging to core and shell layers of the particles as follows:

$$O_c = \frac{N_c}{N_c + N_{sh}}Q_c, \qquad O_{sh} = \frac{N_{sh}}{N_c + N_{sh}}O_{sh}. \tag{4}$$

In addition, we calculate the time average of the energy of the particles as follows [47]:

$$E_{tot} = -\frac{w}{2\pi(N_c + N_{sh})}\oint \hat{H}dt \tag{5}$$

By benefiting from Eq. (5), the specific heat can be obtained as:

$$C = \frac{dE_{tot}}{dT}, \tag{6}$$

where T denotes the absolute temperature. Here we should mention that dynamical phase diagrams are presented by benefiting from the peaks of heat capacities.

3. Results and discussion

It is known that, depending on the value of period τ and reduced amplitude h_0/J_{sh} of the external applied field, the magnetic system can exist in a dynamically ordered or disordered phase. In other words, the dynamic phase boundary line separating the ordered and disordered phases strongly depends on the applied field components as well as other system parameters. Keeping this in mind, for spherical and cubical magnetic nanoparticles, we give the dynamic phase boundaries in the $(J_{int}/J_{sh} - T_c/J_{sh})$ plane with three oscillation period values $\tau = 50,\ 100$, and 200 for some selected values of reduced field amplitudes such as $h_0/J_{sh} = 0.0,\ 0.25$, and 0.5 in Figures 2a–2c. Here, the reduced FM coupling parameter is selected to be $J_c/J_{sh} = 0.75$.

At first glance, one can clearly deduce from Figures 2a–2c that dynamically ordered regions expand with decreasing values of the field amplitude for all considered periods for both spherical and cubical particles. It is also found that the phase transition temperatures of the particles explicitly depend on their geometrical structures as well as system parameters. For example, in relatively small AFM coupling regions, the cubical particle has a higher transition temperature than the spherical one. With increasing strength of the AFM interface coupling $J_{int}/J_{sh} \quad T_c$ values of both particles gradually increase, and after a certain value of J_{int}/J_{sh}

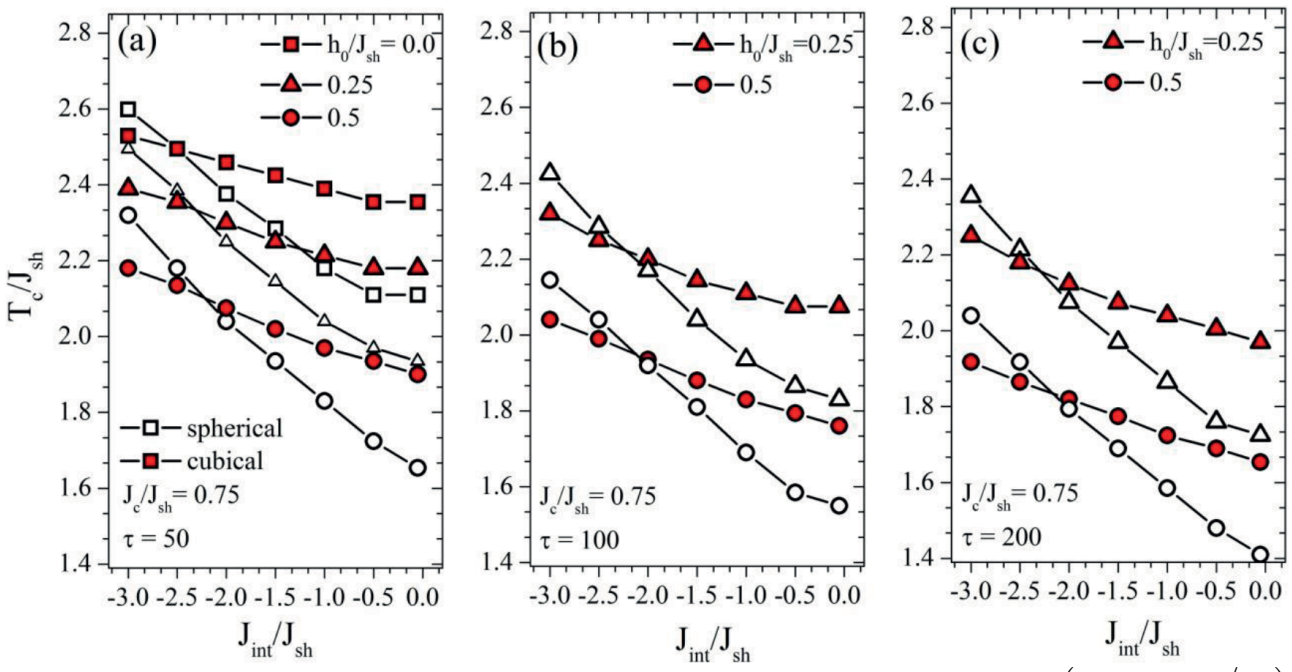

Figure 2. Dynamic phase boundaries of the cubical and spherical nanoparticle systems in the $\left(J_{int}/J_{sh} - T_c\Big/J_{sh}\right)$ planes for value of $J_c\Big/J_{sh} = 0.75$ at various values of the field amplitude $h_0\Big/J_{sh} = 0.0,\ 0.25$, and 0.5. The diagrams are given for (a) $\tau = 50$, (b) $\tau = 100$, and (c) $\tau = 200$.

the transition temperature of the spherical particle becomes larger than that of the cubical one. It is also possible to emphasize that the transition temperatures of particles get lower with an increment of τ The physical mechanism underlying of this observation can be found in reference [51].

Moreover, for weak $|J_{int}/J_{sh}|$ values, core and shell layers of the particles become nearly independent of each other. As the strength of the AFM interaction is enhanced, it becomes dominant against the periodic local fields, and the particle exhibits a strong FM order. Hence, a relatively large amount of thermal energy is needed to observe a dynamic phase transition in the system, due to the response of the spins to the external magnetic field. As a result, dynamically ferrimagnetic ordered phase regions in the phase diagrams shown in Figures 2a–2c become narrower with increasing h_0 and τ values.

In order to understand in detail the influences of the J_{int}/J_{sh} parameters on the temperature dependencies of heat capacities corresponding to the phase diagram depicted in Figure 2a, we plot the thermal variations of heat capacities for relatively low and high values of J_{int}/J_{sh} in Figures 3a and 3b for selected values of Hamiltonian parameters such as $J_c/J_{sh} = 0.75$ $h_0/J_{sh} = 0.25$, and $\tau = 50$. It is possible to figure out from the curves that dynamic heat capacities present a hump behavior located at the relatively low temperature regions and a sharp peak corresponding to the dynamic phase transition point. Our calculations indicate that the hump behaviors are a result of a sudden change in the core magnetizations. This type of observation was also reported in our recent MC studies [50,51]. We should note that the positions of the sharp peaks definitively depend on the AFM coupling parameter as well as the geometrical structures of nanoparticles with similar sizes.

In Figures 4a–4d, we depict the thermal variations of dynamic order parameters of cubical and spherical nanoparticles corresponding to phase diagrams plotted in Figure 2a for various AFM exchange coupling param-

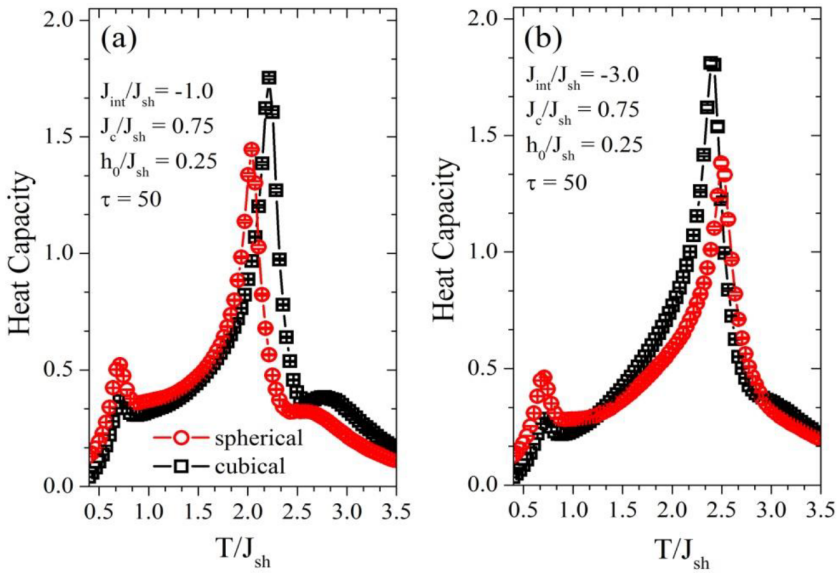

Figure 3. Effects of the AFM interface coupling parameter on the heat capacities of spherical and cubical magnetic nanoparticle systems corresponding to the phase diagrams depicted in Figure 2a.

eters with selected applied field amplitude $h_0/J_{sh} = 0.25$ and period $\tau = 50$. Based on the upper left panel in Figure 4, it can be easily said that when temperature increases, starting from zero, both cubic and spherical nanoparticle systems demonstrate unusual and interesting behaviors. For instance, they show a temperature-induced local maximum in the low temperature region and, with an increment in temperature value, each of the particles exhibits a second-order dynamic phase transition between dynamically ordered and disordered phases. Figure 4b illustrates the temperature dependencies of the sublattice magnetizations of cubic and spherical particles. It is possible to mention that even though the FM exchange coupling of the core particles is weaker than that of the shell layer, both the core and shell layers of two particles bring about a dynamic phase transition at the same critical temperature, which is a result of the relatively strong interface coupling. An interesting result occurs with further increment in AFM exchange coupling parameter. As seen in the magnetization curves shown in Figures 4c and 4d, the phase transition temperature of the spherical particle becomes larger than the cubic one. Additionally, the sudden changes in the core magnetizations of both particles arise with increasing temperature, and, as we mentioned above, these changes give rise to the existence of local humps located at relatively small temperatures depending on the Hamiltonian parameters in the thermal variations of heat capacities.

In the following analysis, let us investigate the influences of the applied field amplitude h_0/J_{sh} on the dynamic order parameter curves of the spherical and cubical nanoparticles, corresponding to the phase diagrams depicted in Figure 2b for considered values of Hamiltonian parameters such as $J_{int}/J_{sh} = -0.5$, $J_c/J_{sh} = 0.75$, and $\tau = 100$. In Figures 5a and 5b, we represent the thermal variations of total magnetization curves with varying values of h_0/J_{sh}

It is possible to say that dynamic evolutions of spherical and cubical particles strongly depend on the amplitude of the external applied field. As seen in these figures, the phase transition temperatures of the particles decrease with increasing h_0/J_{sh} values. The related physical mechanism can be understood via a Landau-type double well potential [39,45].

In Figures 6a and 6b, we show the influences of the external field period τ on the dynamic phase transition

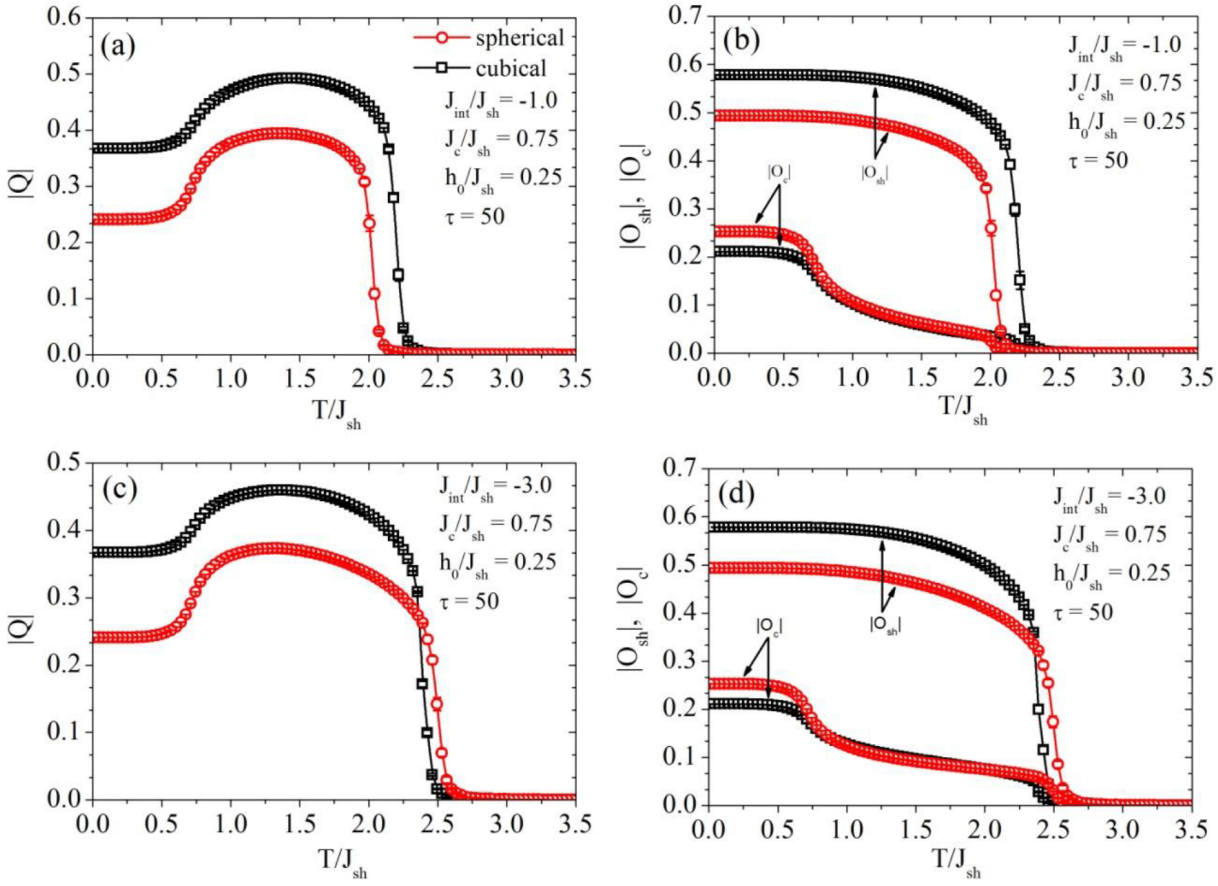

Figure 4. Effect of the AFM interface coupling parameter on the temperature dependencies of order parameter Q, O_{sh}, and O_c of spherical and cubic magnetic nanoparticle systems for parameters corresponding to the phase diagrams depicted in Figure 2a.

characteristics of the particles. One can easily show that the thermal variations of the dynamic order parameters of both spherical (6a) and cubical (6b) particles are very sensitive to the applied field period, and with increasing period, the phase transition temperatures of both particles decrease for the considered Hamiltonian parameters. The physical facts underlying these findings observed in Figures 6a and 6b are identical to those emphasized in Figures 2a–2c. Therefore, we will not discuss these interpretations here.

As a final investigation, we focus our attention upon the coercivity and hysteresis behaviors of cubical and spherical magnetic nanoparticles. At this point, we want to underline that there exist clear differences between dynamic and static hysteresis behaviors. It is beneficial to directly talk about the properties of dynamic hysteresis, since the static hysteresis mechanism of equilibrium systems is well known from the previous comprehensive investigations [71]. Dynamic hysteresis occurs because of the dynamic phase lag between time-dependent magnetization and the applied oscillating magnetic field. In a magnetic system under the influence of an oscillating magnetic field, the hysteresis behaviors can be classified into two classes by seeing the shapes of the dynamic hysteresis curves: in the first class, the system exhibits symmetric hysteresis loops around the origin corresponding to the dynamically disordered phase, whereas it is possible to see asymmetric hysteresis loops corresponding to the ordered phase in the second class. Moreover, by benefiting from the coercivity and remanent magnetization of the system, the geometrical shape of the hysteresis loop can be determined.

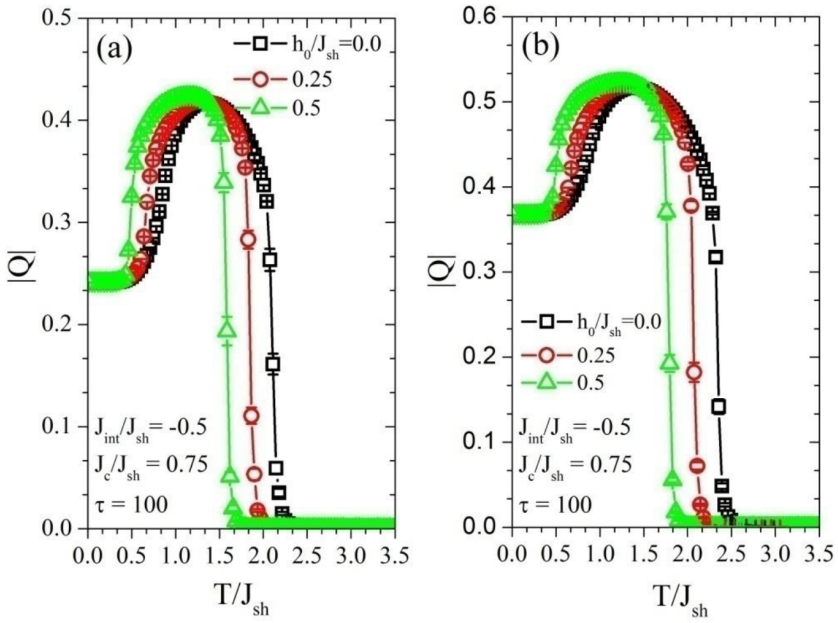

Figure 5. Thermal variations of the dynamic order parameters Q of spherical (a) and cubical (b) magnetic nanoparticle systems with varying $h_0 \big/ J_{sh}$ for selected values of Hamiltonian parameters such as $J_{int} \big/ J_{sh} = -0.5$, $J_c \big/ J_{sh} = 0.75$, and $\tau = 100$.

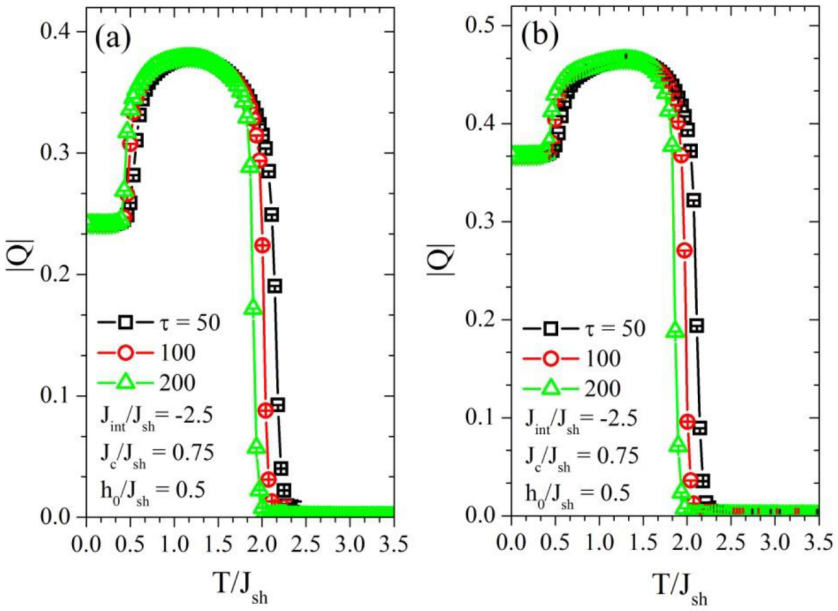

Figure 6. Applied field period τ dependencies of the thermal variations of the dynamic order parameters Q of spherical (a) and cubical (b) magnetic nanoparticle systems for selected values of Hamiltonian parameters such as $J_{int} \big/ J_{sh} = -2.5$, $J_c \big/ J_{sh} = 0.75$, and $h_0 \big/ J_{sh} = 0.5$.

In Figures 7a, 7b, 8a, and 8b, we give the applied field period and amplitude dependencies of the coercivity and dynamic hysteresis loops for cubical and spherical magnetic nanoparticle systems, respectively.

The hysteresis simulation procedure is defined briefly as follows: the dynamic hysteresis loops are calculated at a special temperature $T = 0.8T_c^0$, where T_c^0 is the equilibrium transition temperature of the system. This type of choice of temperature has been done in some of the previously published studies concerning the dynamic phase transition properties of different types of magnetic systems [46,50–52], and it is obvious from the studies that at such a temperature one can easily observe a purely oscillating magnetic field induced phase transition between dynamically ordered and disordered phases.

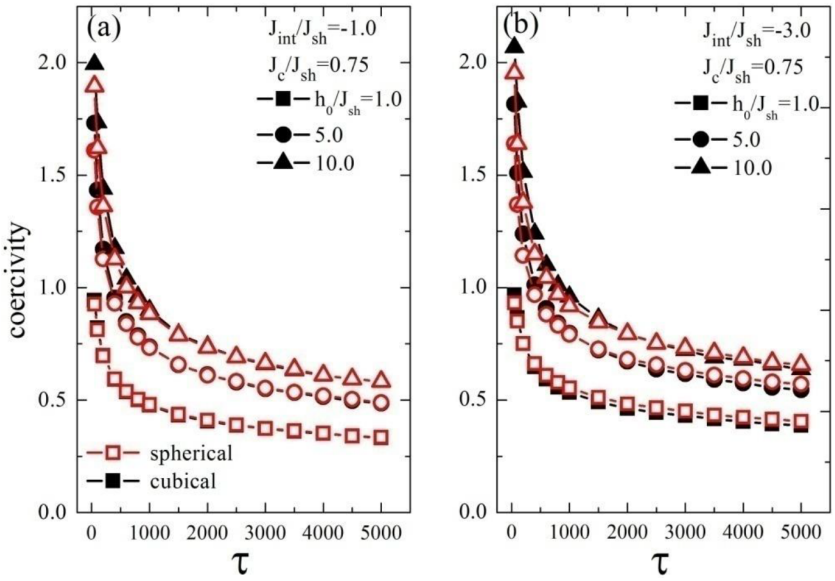

Figure 7. Variations of the coercive fields as a function of the oscillation period for several values of $h_0 \Big/ J_{sh}$ with $J_c \Big/ J_{sh} = 0.75$ and (a) $J_{int} \Big/ J_{sh} = -1.0$ for (b) $J_{int} \Big/ J_{sh} = -3.0$, respectively.

For these calculations, the first 100 cycles of the external field have been discarded and the data were collected for 400 cycles. After that, by making use of the right-hand (h_c^+) and left-hand (h_c^-) branches of the observed hysteresis loops, the coercivity value $h_c = (h_c^+ - h_c^-)/2$ was obtained for the considered system parameters.

To investigate the effect of the AFM coupling parameter on coercivity profiles of the cubical and spherical magnetic nanoparticles, we give the period dependencies of coercivities at various oscillating field amplitudes in Figures 7a and 7b. It can be said by focusing on Figure 7a that, depending on the applied field amplitudes, it is possible to observe large coercive fields at low applied field periods for both particles. Moreover, it is found that the coercivity curves of two particles exhibit sudden variations with increasing applied field period, whereas for sufficiently high τ they exhibit a stable behavior. Additionally, cubical and spherical particles show almost the same behavior for $J_{int}/J_{sh} = -1.0$. As seen in Figure 7b, an increment in the AFM coupling parameter does not lead to the existence of the very different hysteretic behaviors observed in Figure 7a.

In Figures 8a and 8b, we present the dynamic hysteresis loops corresponding to Figures 7a and 7b for some selected applied field periods with the considered value of $h_0/J_{sh} = 1.0$. It can be deduced from Figures 8a and 8b that the hysteresis loops of both cubical and spherical particles are symmetric in the magnetization versus magnetic field plane and also the remanent magnetization values of the particles do not tend to change when τ varies. Furthermore, the width of the loops of particles becomes narrower but does not vanish for high

τ values, and these situations explicitly indicate the existence of dynamically disordered phases for the selected Hamiltonian parameters. Our kinetic MC simulation investigations highlight that although the general profiles found in Figures 8a and 8b resemble each other, the cubical particle has a relatively larger coercivity value than the cubical one.

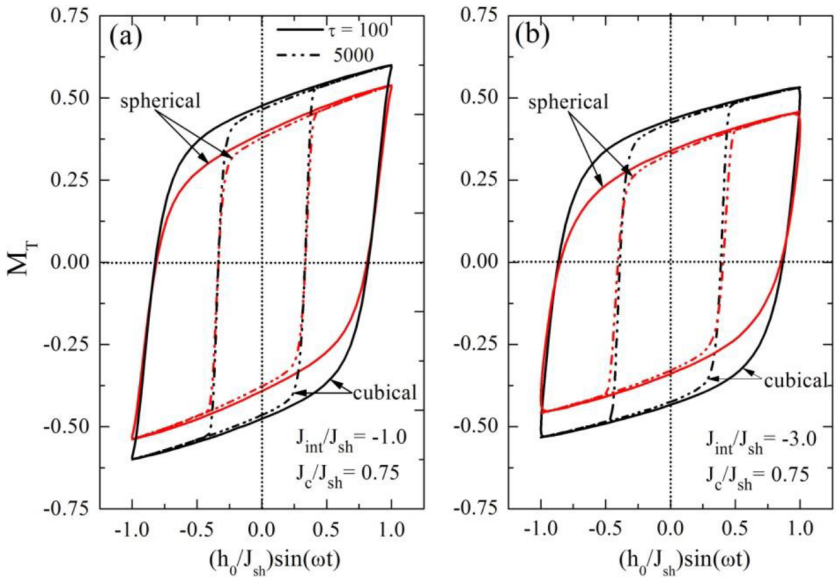

Figure 8. Hysteresis loops of the particles corresponding to Figures 7a and 7b for considered relatively low and high applied field periods.

4. Concluding remarks

In conclusion, based on the standard Metropolis algorithm, we have carried out MC simulations of cubical and spherical magnetic nanoparticles with similar volumes under a time-dependent oscillating magnetic field in order to elucidate how the amplitude and period of the external oscillating magnetic field as well as exchange couplings affect the dynamic critical behaviors of the particles. After a detailed analysis, for both cubical and spherical particles, the dynamic phase boundaries separating the dynamically ordered and disordered phases have been constructed in the $(J_{int}/J_{sh} - T_c/J_{sh})$ plane with selected Hamiltonian parameters. It was found that dynamic evolutions of magnetic nanoparticles explicitly depend on their geometrical shapes as well as Hamiltonian parameters. For fixed sets of values of amplitude and period of the oscillating magnetic field, the cubical one has higher transition temperature than the spherical one for a relatively small interface coupling parameter, whereas the transition temperature of the spherical particle becomes higher than that of the cubical one with further increment in AFM coupling parameter. It was also observed that dynamic heat capacities of particles exhibit a hump behavior originating from a sudden change in the core magnetizations located at the relatively low temperature regions and a sharp peak corresponding to the dynamic phase transition point. In addition to these, we have touched upon the coercivity and hysteresis behaviors of particles, and we found that the coercivities of particles seem to be similar for the relatively low AFM exchange coupling between core and shell spins, whereas some explicit differences, especially in the high applied field period regions, begin to emerge with increasing AFM exchange coupling. It was also demonstrated that both cubical and spherical particles have similar hysteresis shapes for some combinations of Hamiltonian parameters.

All of the observations found in this work show that the Ising model can be successfully applied to such

types of nonequilibrium systems in the presence of a time-dependent forcing magnetic field. However, core-shell nanoparticles have strong surface disorder due to the broken symmetry and roughness; thus, the true nature of the physical facts reported in this work may be further understood with a more realistic model such as the Heisenberg type of Hamiltonian. Clarifying these types of effects on small-sized magnetic nanoparticles will be beneficial for a better understanding of the heat capacity, coercivity, remanence, and other magnetic properties. We think that such a detailed investigation may be an interesting subject of future work. As a final conclusion, we note that more work is required to match and understand the theoretical and experimental findings regarding the thermal and magnetic properties of the advanced functional core-shell nanoparticles in different geometries.

Acknowledgment

The numerical calculations reported in this paper were performed at the TÜBİTAK ULAKBİM High Performance and Grid Computing Center (TRUBA Resources).

References

[1] Ruhrig, M.; Khamsehpour, K. J.; Kirk, J. N.; Chapman, P.; Aitchison, M.; McVitie, S.; Wilkinsons, C. D. W. *IEEE T. Magn.* **1996**, *32*, 4452-4457.

[2] Schrefl, T.; Fidler, J.; Kirk, K. J.; Chapman, J. N. *J. Magn. Magn. Mater.* **1997**, *175*, 193-204.

[3] Fan, Z.; Lu, J. G. *International Journal of High Speed Electronics and Systems* **2006**, *16*, 883-896.

[4] Su, Y. C.; Skomski, R.; Sorge, K. D.; Sellmyer, D. J. *Appl. Phys. Lett.* **2004**, *84*, 1525-1527.

[5] Margeat, O.; Tran, M.; Spasova, M.; Farle, M. *Phys. Rev. B* **2007**, *75*, 134610.

[6] Puntes, V.; Krishnan, K.; Alivisatos, A. *Science* **2001**, *291*, 2115-2117.

[7] Park, J.; An, K.; Hwang, Y.; Park, J. G.; Noh, H. J.; Kim, Y. J.; Park, J. H.; Hwang, N. M.; Hyeon, T. *Nat. Mater.* **2004**, *3*, 891-895.

[8] Niu, X.; Stagon, S. P.; Huang, H.; Baldwin, J. K.; Misra, A. *Phys. Rev. Lett.* **2013**, *110*, 136102.

[9] Cozzoli, P.; Snoeck, E.; Garcia, M.; Giannini, C.; Guagliardi, A.; Cervellino, A.; Gozzo, F.; Hernando, A.; Achterhold, K.; Ciobanu, N. et al. *Nano Lett.* **2006**, *6*, 1966-1972.

[10] Roca, A.; Morales, M.; O'Grady, K.; Serna, C. *Nanotechnology* **2006**, *17*, 2783-2788.

[11] Berkowitz, A. E.; Kodama, R. H.; Makhlouf, S. A.; Parker, F. T.; Spada, F. E.; McNiff, E. J. Jr.; Foner, S. *J. Magn. Magn. Mater.* **1999**, *196*, 591-594.

[12] Pankhurst, Q. A.; Connolly, J.; Jones, S. K.; Dobson, J. *J. Phys. D* **2003**, *36*, R167-R181.

[13] Rivas, J.; Bonobre-Lopez, M.; Pineiro-Redondo, Y.; Rivas, B.; Lopez-Quintela, M. A. *J. Magn. Magn. Mater.* **2012**, *324*, 3499-3502.

[14] Ivanov, Y. P.; Alfadhel, A.; Alnassar, M.; Perez, J. E.; Vazquez, M.; Chuvilin, A.; Kosel, J. *Sci. Rep.* **2016**, *6*, 24189.

[15] Bader, S. D. *Rev. Mod. Phys.* **2006**, *78*, 1.

[16] Kittel, C. *Phys. Rev.* **1946**, *70*, 965-971.

[17] Chudnovsky, E. M.; Gunther, L. *Phys. Rev. Lett.* **1988**, *60*, 661-664.

[18] Kneller, E. F.; Luborsky, F. E. *J. Appl. Phys.* **1963**, *34*, 656-658.

[19] Nogues, J.; Sort, J.; Langlais, V.; Skumryev, V.; Surinach, S.; Munoz, J. S.; Baro, M. D. *Phys. Rep.* **2005**, *422*, 65-117.

[20] Iglesias, O.; Labarta, A.; Batlle, X. *J. Nanosci. Nanotechnol.* **2008**, *8*, 2761-2780.

[21] Leite, V. S.; Figueiredo, W. *Physica A* **2005**, *350*, 379-392.

[22] Leite, V. S.; Figueiredo, W. *Phys. Lett. A* **2008**, *372*, 898-903.

[23] Kaneyoshi, T. *J. Magn. Magn. Mater.* **2009**, *321*, 3430-3435.

[24] Kaneyoshi, T. *Phys. Stat. Sol. B* **2005**, *242*, 2938-2948.

[25] Wang, C. D.; Lu, Z. Z.; Yuan, W. X.; Kwok, S. Y.; Teng, B. H. *Phys. Lett. A* **2011**, *375*, 3405-3409.

[26] Keskin, M.; Sarli, N.; Deviren, B. *Sol. Stat. Commun.* **2011**, *151*, 1025-1030.

[27] Zaim, A.; Kerouad, M.; Boughrara, M. *J. Magn. Magn. Mater.* **2013**, *331*, 37-44.

[28] Garanin, D. A.; Kachkachi, H. *Phys. Rev. Lett.* **2003**, *90*, 065504

[29] Wesselinowa, J. M. *J. Magn. Magn. Mater.* **2010**, *322*, 234-237.

[30] Leite, V. S.; Grandi, B. C. S.; Figueiredo, W. *Phys. Rev. B* **2006**, *74*, 094408.

[31] Berger, L.; Labaye, Y.; Tamine, M.; Coey, J. M. D. *Phys. Rev. B* **2008**, *77*, 104431.

[32] Hu, Y.; Du, A. *J. Appl. Phys.* **2007**, *102*, 113911.

[33] Vasilakaki, M.; Trohidou, K. N. *Phys. Rev. B* **2009**, *79*, 144402.

[34] Zaim, A.; Kerouad, M.; El Amraoui, Y. *J. Magn. Magn. Mater.* **2009**, *321*, 1077-1083.

[35] Zaim, A.; Kerouad, M. *Physica A* **2010**, *389*, 3435-3442.

[36] Jiang, L.; Zhang, J.; Chen, Z.; Feng, Q.; Huang, Z. *Physica B* **2010**, *405*, 420-424.

[37] Yüksel, Y.; Aydiner, E.; Polat, H. *J. Magn. Magn. Mater.* **2011**, *323*, 3168-3175.

[38] Iglesias, O.; Labarta, A. *J. Magn. Magn. Mater.* **2004**, *272-276*, 685-686.

[39] Chakrabarti, B. K.; Acharyya, M. *Rev. Mod. Phys.* **1999**, *71*, 847-859.

[40] Acharyya, M. *Int. J. Mod. Phys. C* **2005**, *16*, 1631-1670.

[41] Park, H.; Pleimling, M. *Phys. Rev. Lett.* **2012**, *109*, 175703.

[42] Tomè, T.; de Oliveira, M. J. *Phys. Rev. A* **1990**, *41*, 4251-4254.

[43] Lo, W. S.; Pelcovits, R. A. *Phys. Rev. A* **1990**, *42*, 7471-7474.

[44] Acharyya, M. *Phys. Rev. E* **1998**, *58*, 179-186.

[45] Acharyya, M.; Chakrabarti, B. K. *Phys. Rev. B* **1995**, *52*, 6550-6568.

[46] Acharyya, M. *Physica A* **1998**, *253*, 199-204.

[47] Acharyya, M. *Phys. Rev. E* **1997**, *56*, 2407-2411.

[48] Sides, S. W.; Rikvold, P. A.; Novotny, M. A. *Phys. Rev. E* **1999**, *59*, 2710-2729.

[49] Park, H.; Pleimling, M. *Phys. Rev. E* **2013**, *87*, 032145.

[50] Yüksel, Y.; Vatansever, E.; Polat, H. *J. Phys.: Condens. Mat.* **2012**, *24*, 436004.

[51] Vatansever, E.; Polat, H. *J. Magn. Magn. Mater.* **2013**, *343*, 221-227.

[52] Wu, M. H.; Dong, S.; Liu, J. M. *J. Appl. Phys.* **2008**, *103*, 07B103.

[53] Acharyya, M. *J. Phys. A-Math. Gen.* **1994**, *27*, 1533-1540.

[54] Punya, A.; Yimnirun, R.; Laoratanakul, P.; Laosiritaworn, Y. *Physica B* **2010**, *405*, 3482-3488.

[55] Shi, X.; Wei, G.; Li, L. *Phys. Lett. A* **2008**, *372*, 5922-5927.

[56] Deviren, B.; Keskin, M. *Phys. Lett. A* **2012**, *376*, 1011-1019.

[57] Deviren, B.; Kantar, E.; Keskin, M. *J. Magn. Magn. Mater.* **2012**, *324*, 2163-2170.

[58] Yüksel, Y.; Vatansever, E.; Akinci, U.; Polat, H. *Phys. Rev. E* **2012**, *85*, 051123.

[59] Glauber, R. J. *J. Math. Phys.* **1963**, *4*, 294-307.

[60] Nèel, L. *Ann. Phys.* **1948**, *3*, 137-198.

[61] Strecka, J. *Physica A* **2006**, *360*, 379-390.

[62] Song, Q.; Zhang, Z. J. *J. Am. Chem. Soc.* **2004**, *126*, 6164-6168.

[63] Seo, W.; Jo, H.; Lee, K.; Kim, B.; Oh, S.; Park, J. *Angew. Chem. Intl. Ed.* **2004**, *116*, 1135-1137.

[64] Dimitrov, D. A.; Wysin, G. M. *Phys. Rev. B* **1994**, *50*, 3077-3084.

[65] Evans, R.; Nowak, U.; Dorfbauer, F.; Shrefl, T.; Mryasov, O.; Chantrell, R. W.; Grochola, G. *J. Appl. Phys.* **2006**, *99*, 08G703.

[66] Yanes, R.; Chubykalo-Fesenko, O.; Kachkachi, H.; Garanin, D. A.; Evans, R.; Chantrell, R.W. *Phys. Rev. B* **2007**, *76*, 064416.

[67] Bai, J.; Xu, Y.; Wang, J. *IEEE T. Magn.* **2007,** *43*, 3340-3342.

[68] Salaver-Alvarez, G.; Qin, J.; Sepelak, V.; Bergmann, I.; Vasilakaki, M.; Trohidou, K. N.; Ardisson, J. D.; Macedo, W. A. A.; Mikhaylova, M.; Muhammed, M. et al. *J. Am. Chem. Soc.* **2008**, *130*, 13234-13239.

[69] Binder, K. *Monte Carlo Methods in Statistical Physics*; Springer: Berlin, Germany, 1979.

[70] Newman, M. E. J.; Barkema, G. T. *Monte Carlo Methods in Statistical Physics*; Clarendon Press: Oxford, UK, 2001.

[71] Bertotti, G. *Hysteresis in Magnetism: For Physicists, Materials Scientists, and Engineers*; Elsevier: Amsterdam, the Netherlands, 1998.